# Seaweed to Dendrite Transition in Directional Solidification

Nikolas Provatas,[1] Quanyong Wang,[2] Mikko Haataja,[3] and Martin Grant[2]

[1]*McMaster University, Department of Materials Science and Engineering, 1280 Main Street West, Hamilton, Ontario, Canada, L8S 4L7*

[2]*McGill University, Department of Physics, 3600 University, Montréal, Québec, Canada, H3A 2T8*

[3]*Princeton University, Department of Mechanical and Aerospace Engineering, Princeton, New Jersey 08544, USA*

(Received 31 May 2003; published 10 October 2003)

We simulate directional solidification using a phase-field model solved with adaptive mesh refinement. For small surface tension anisotropy directed at 45° relative to the pulling direction we observe a crossover from a seaweed to a dendritic morphology as the thermal gradient is lowered, consistent with recent experimental findings. We show that the morphology of crystal structures can be unambiguously characterized through the local interface velocity distribution. We derive semiempirically an estimate for the crossover from seaweed to dendrite as a function of thermal gradient and pulling speed.

DOI: 10.1103/PhysRevLett.91.155502 PACS numbers: 81.30.Fb, 68.70.+w

The study of solidification microstructures is fundamental to many problems of scientific and practical significance. Among these is the optimization of metal alloys, the properties of which depend on their microstructure [1,2]. In traditional casting, microstructure is formed through solidification and thermomechanical processing, which typically destroys the initial as-cast structure. In emerging technologies, such as *strip casting*, thin alloy strips are rapidly cooled with little thermomechanical treatment. In these materials, the final microstructure is largely governed by the physics of solidification.

The fundamental solidification structure is the dendrite. Dendrites can be grown in isolation, where their growth rate is selected by a solvability criterion that is established due to a singular perturbation in the surface tension anisotropy [3,4]. In casting applications solidification occurs as a competitive growth of multiple arrays, often growing as an advancing front, directionally solidified in a thermal gradient established by heat flow out of a cast.

A paradigm used to study solidification in a 2D geometry — a phenomenon with many parallels in strip casting — is *directional solidification*. In this process a material is solidified while being pulled through a unidirectional temperature gradient $G$ at a velocity $v$. The solidification front becomes unstable by the Mullins-Sekerka instability [5], leading to a variety of complex cell and dendrite patterns. A long-standing problem has been to elucidate the mechanism of wavelength selection in such cellular or dendritic arrays. This problem has been extensively examined experimentally [6–15], and theoretically [6,10,16–20] using boundary integral methods, phase-field models, and semiempirical thermodynamic considerations.

Another class of directionally solidified microstructures recently examined experimentally [6,15] and numerically [6,21] is known as *seaweed*. These structures are formed through successive tip splitting of primary branches of the solidification front. Surviving tips grow and continue to split, while trailing branches become subsumed by neighbor interactions. Seaweed can emerge when the direction of solidification is tilted at an angle with respect to the direction of a small surface tension anisotropy. Of particular importance is the recent experimental observation [15] that when the thermal gradient is reduced, there is a morphological transition from seaweed to directed dendritic structures that lock into the symmetric anisotropy directions. It has been conjectured that this transition is an effect of the finite surface tension anisotropy [15]. The precise mechanism of this morphological transition remains unexplained, however. Understanding how the thermal gradient, pulling speed, and crystalline anisotropy control dendritic growth is critical in predicting solidification microstructures in polycrystalline materials.

In this Letter, we report simulations that examine the crossover mechanism for the seaweed to dendrite transition reported in Ref. [15]. We use a phase-field model solved on an adaptive grid, gaining access to systems with reduced finite size effects, a factor which has traditionally plagued studies where the size of the system is on the order of the diffusion length. We find a morphological transformation from seaweed to directed dendritic growth as the thermal gradient is decreased. The crossover transition is shown to be well characterized through the local interface velocity distribution function. We then derive a semianalytic phase diagram of seaweed versus dendrite growth as a function of pulling velocity and thermal gradient.

We model directional solidification with a phase-field model of an ideal binary alloy with parallel solidus and liquidus slopes [17,20]. The model couples an order parameter $\phi$ to a concentration field $C$. The field $\phi(\vec{x})$ takes on the values $\phi = -1$ in the solid phase, $\phi = 1$ in the liquid phase, and interpolates continuously between these states in the interface region. The field $C$ is normalized to the concentration gap $\Delta C$. In units where space is scaled by $W_o$, the interface width, and time by $\tau_o$, the interface

  

kinetics time, the equations of motion for the two fields are given by

$$\frac{\partial C}{dt} = D\nabla \cdot [q(\phi)\nabla\mu] + v_p \frac{\partial C}{\partial z}$$

and

$$A^2(\vec{n})\frac{\partial \phi}{dt} = \vec{\nabla} \cdot [A^2(\vec{n})\vec{\nabla}\phi] + \phi(1-\phi^2) + (\lambda\mu + U)(1-\phi^2)^2 + \frac{1}{2}\vec{\nabla} \cdot \left[ |\nabla\phi|^2 \frac{\partial A^2(\vec{n})}{\partial(\vec{\nabla}\phi)} \right] + v_p \frac{\partial \phi}{\partial z},$$

where $\mu = C - P(\phi)/2$, $P(\phi) = (15/8)(\phi - 2\phi^3/3 + \phi^5/5)$ and the equations have been written in a frame of reference moving with the pulling velocity $v_p = (v_s\tau_o)/W_o$, where $v_s$ is the dimensional pulling speed. The two fields are coupled via the constant $\lambda$. The dimensionless diffusion constant is $D = D_L\tau_o/W_o^2$, where $D_L$ is the diffusion constant in the liquid. Two-sided diffusion is controlled by $q(\phi) = 1/\{Q_1 + Q_2[\phi + b(1 - |\phi|)]\}$ [22], where $Q_1$ and $Q_2$ are selected such that the ratio of solid to liquid diffusion constants $D_s/D = \xi = 0.1$, and $b$ is a constant (specified below). Temperature is prescribed by a *frozen field* $U = \Delta T_o + G_m z$, where $z$ is the pulling direction and $G_m = G\lambda W_o/\Delta C M_L$, with $G$ the thermal gradient, $M_L$ the liquidus slope, and $T_o(= 0)$ a reference temperature. Surface tension anisotropy is defined in terms of $\vec{n} = \vec{\nabla}\phi/|\nabla\phi|$, the unit normal to the contours of $\phi$. Specifically, $A(\vec{n}) = [1 - 3\epsilon_4][1 + \frac{4\epsilon_4}{1-3\epsilon_4}((n_x)^4 + (n_y)^4)]$, where $\epsilon_4$ is the anisotropy constant. The anisotropic interface width is thus defined as $W(\vec{n}) = W_o A(\vec{n})$ and the characteristic time $\tau(\vec{n}) = \tau_o A^2(\vec{n})$ [23–25].

The constants $W_o$, $\tau_o$, $\lambda$, and $b$ are interrelated by an asymptotic analysis [26] which maps the phase-field model onto the sharp interface limit defined by (1) solute diffusion in the bulk phases, (2) flux conservation at phase boundaries, and (3) the Gibb's Thomson condition $C_{\text{int}} - C_{\text{eq}} = -d(\vec{n})\kappa - \beta(\vec{n})v$, with $\kappa$ the local interface curvature, $d(\vec{n}) = d_o[A(\vec{n}) + \partial^2 A/\partial(\cos^{-1}n_x)^2]$, where $d_o$ is the isotropic capillary length, and $v$ is the local interface speed. In the limit $\beta = 0$, we obtain $b = 0.925$, $d_o/W \approx 0.471/\lambda$, and $D \approx 1.92\lambda$. We note that our results will also hold qualitatively for a wider range of phase-field parameters.

The phase-field model was simulated using a finite element method on an adaptive grid, with zero-flux boundary conditions in both $C$ and $\phi$ as in Ref. [28]. Solidification is initiated by a small-amplitude, randomly perturbed solid/liquid interface. The initial solute profile $C(\vec{x}, 0)$ was set to a steady-state diffusion profile normal to the interface, while $\phi(\vec{x}, 0) = \tanh[\vec{x}/\sqrt{(2)}]$ along the normal to the interface. The system size was $4092 \times 4092$ with a minimum grid spacing of $dx_{\min} = 0.5$. We note that simulations with larger $dx = 1$ also reproduce our results, with a small shift in the corresponding critical thermal gradient ($\Delta G_m \approx 0.0002$) for ranges of anisotropy examined. Also, simulations in smaller systems ($1024 \times 1024$) do not clearly exhibit the crossover transition from seaweed to dendrites, while doubling the system size to $8196 \times 8196$ leads to the same results as those in the $4092 \times 4092$ system. We used explicit time integration, with a time step $dt = 0.01$. The coupling parameter $\lambda = 1$ for all simulations. The dimensionless pulling speed was fixed for all our numerical runs at $v_p = 0.015$, corresponding to $v = 32\ \mu$m/s for a pivalic acid (PVA) 0.04 wt.% acetone alloy. Typical cooling rates examined ranged from 0.014-1 K/s.

We simulated directional solidification with $v_p$ oriented along the $z$ axis and surface tension anisotropy oriented $\theta = 45°$ with respect to $v_p$. For all nonzero anisotropy values examined, cellular structures emerged at large thermal gradients $G_m$. As $G_m$ was lowered, seaweed structures emerged. Figure 1 shows a typical seaweed configuration for $G = 0.001$ and $\epsilon_4 = 0.0075$. This morphology is characterized by successive tip splitting, closely resembling the experimental seaweed of Refs. [6,15]. Lowering $G_m$ further gave rise to dendrites that lock into the anisotropy directions. Figure 2 shows a typical dendritic morphology, similar to the experimental data in Fig. 25 of Ref. [6]. We note that the dendrites in Fig. 2 resemble the experimental branches in Fig. 7a in Ref. [15], which are presented as part of a seaweed, although the branches look dendritic. We found that near the crossover, seaweed branches can resemble dendritic side branches making visual distinction between seaweed or dendrite ambiguous.

Evidence of the crossover between seaweed and dendritic morphology is quantified by examining the interface velocity distribution. Figure 3 shows the distribution of transverse ($x$ direction) velocity ($v_x$) for different $G_m$

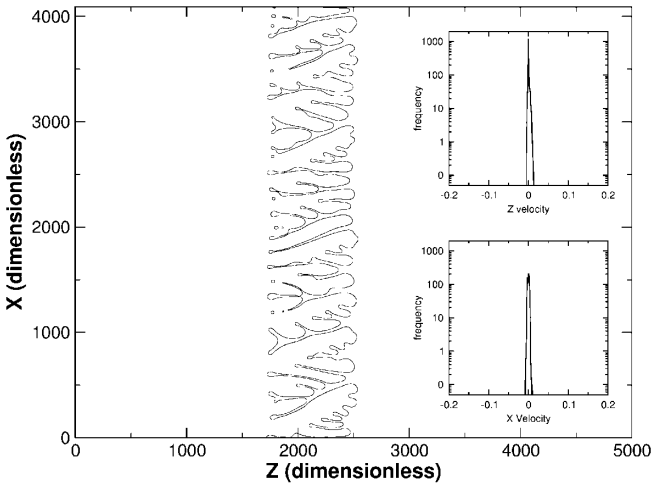


FIG. 1. Seaweed (anisotropy $\epsilon = 0.0075$, thermal gradient $G_m = 0.0008$) is characterized by successive tip splitting. Insets show the distribution of forward (top) and transverse (bottom) interface velocities.

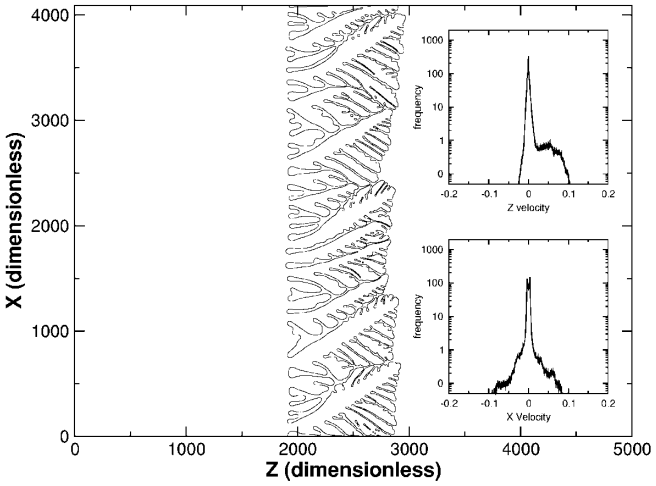


FIG. 2. Oriented dendrites (anisotropy $\epsilon = 0.0075$, thermal gradient $G_m = 0.0002$), growing near the $\theta = \pi/4$ direction. Insets show the distribution of forward (top) and transverse (bottom) interface velocities.

and $\epsilon_4$. Figure 4 shows the corresponding distributions in the pulling direction ($v_z$). The $z$ velocity is biased to the right since the sample is pulled to the left. The distributions represent microstructure development for $t > 1$ s. In all cases, the narrowest distributions correspond to seaweed morphologies. In this regime the relative $z$ velocity of the interface is small, while $x$-direction velocity is limited due to interbranch interactions. As $G_m$ is lowered, large-velocity shoulders begin to appear in both distributions, becoming progressively broader as clearly defined oriented dendrites emerge. The crossover gradient corresponds to $G_m \approx 0.0005$ for $\epsilon_4 \geq 0.005$ and $G_m \approx 0.0003$ for $\epsilon_4 < 0.005$. We note the weak dependence of $G_m$ on $\epsilon_4$. The dimensionless tip undercooling ($\Delta = 1 - z/l_T$, where $l_T = \lambda/G_m$ is the thermal length) was lowest for seaweed and largest for dendrites. This leads to large velocities at low $G_m$ (e.g., $\Delta \approx 0.93$ for $G_m = 0.000\,05$, $\epsilon_4 = 0.001$) and decreasing interbranch spacing, consistent with Mullins-Sekerka theory. At these low values of $G_m$ we are likely observing the effects of the finite-interface thickness and kinetics as the diffusion length is of order the interface thickness, making our results in this regime qualitative. We note, however, that for the anisotropies examined, the crossover transition from seaweed to dendrites always occurred for $G_m$ above the threshold where kinetic or finite-interface effects could be observed. We also note that similar evidence for a crossover was observed if we examine the distribution of local interface-normal angles.

An estimate of the crossover gradient from seaweed to dendritic growth is obtained by noting that the wavelength $\lambda^*$ of a dendritic array tilted at an angle $\theta$

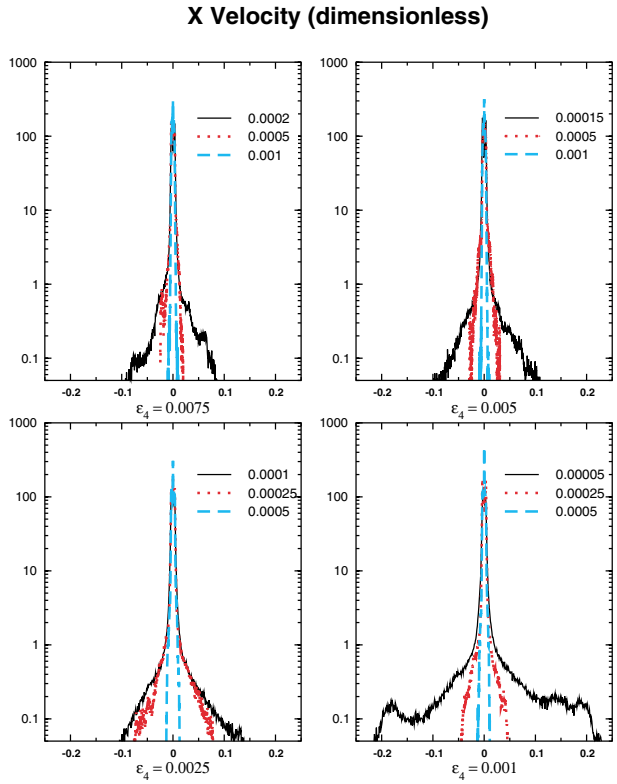


FIG. 3 (color online). Distribution of transverse ($x$ axis) interface velocity for different gradients (shown in the legend). For all $\epsilon_4$, the narrowest distributions correspond to seaweed. The broadening of the distribution corresponds to the emergence of oriented dendrites.

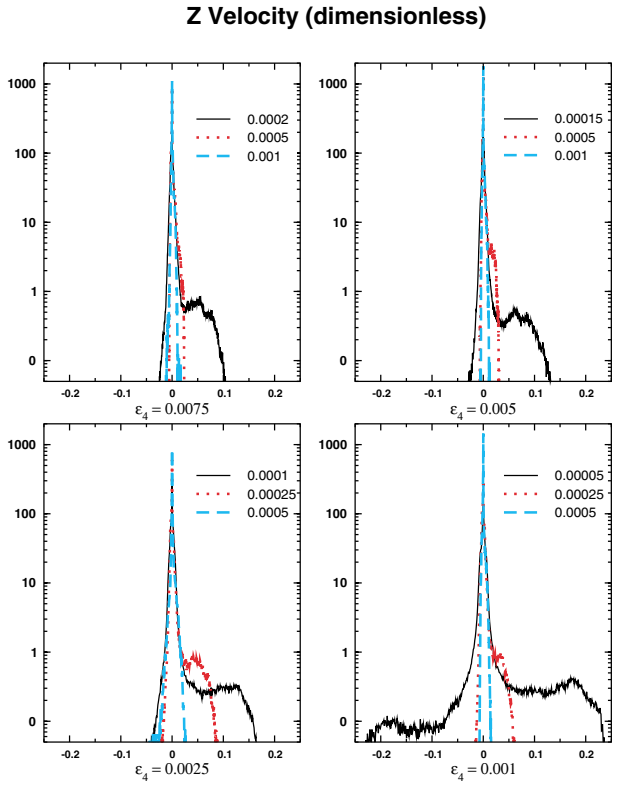


FIG. 4 (color online). Distribution of the local interface velocity in the pulling ($z$ axis) direction corresponding to the data of Fig. 3.

to the $z$ axis must satisfy the selection criterion $\lambda^* = \alpha l_T$, where $\alpha$ is some proportionality constant. This criterion requires that the wavelength of a tilted dendritic array must scale with $l_T$, which determines the maximum amplitude of a dendritic protrusion along the growth direction. For the form of $\lambda^*$ we follow Ref. [9], which finds experimentally that the wavelength of a dendritic array $\lambda^* \propto (\overline{d}_o l_D l_T)^{1/3}$, where $\overline{d}_o(\theta) = d_o(1 + 15\epsilon_4 \cos(4\theta))$ and $l_D = 2D/(v_p \cos\theta)$, with $v_p \cos\theta$ representing the average normal velocity of the array at steady state. The constant $\alpha$ is estimated using the additional information that the onset of dendritic morphology occurs when $l_T/l_D \approx 8$ (consistent with other work [6,29]). Using this to eliminate $l_T$ in the onset criterion above gives $\alpha \approx 0.03$. Replacing $\alpha$ in the selection criterion finally gives $G^* \approx P_f \sqrt{(v_p \cos\theta)/(D d_o(1 - 15\epsilon_4 \cos 4\theta))}$ with $P_f = 0.004$. For our fixed velocity of $v_p = 0.015$, $\theta = \pi/4$, and $\epsilon_4 = 0.005$, our predicted crossover for $G^* \approx 0.000\,45$, consistent with the data of Figs. 3 and 4, which show a crossover just below $G_m \approx 0.0005$. We note that using the form $\lambda^* = (l_T^2 l_D d_o)^{1/4}$ developed by Hunt and Jackson [30] gives the same form for $G^*$, with $P_f = 0.0032$. Fitting the above onset criterion directly to our $\epsilon_4 = 0.005$, $G^* \approx 0.0005$ data by estimating the transient normal velocity from Figs. 3 and 4 gives $P_f = 0.0027$, consistent with the theoretical derivations above.

We can use this selection criterion to define a morphological phase diagram for $G_m(v_p)$ for a fixed $\epsilon_4$. Examination of $G_m(v_p)$ also predicts that there will be a crossover from seaweed to dendrites as $v_p$ is increased, consistent with the findings of [6]. This is expected as $l_D/l_T \to 0$ as $v_p$ increases. We note that at sufficiently large $v_p$ the fastest growing unstable wavelength will always occur in the forward direction regardless of the angle of anisotropy. We therefore only expect $G_m(v_P)$ to be valid at small $v_p$.

To conclude, we have investigated the crossover transition from seaweed structures to tilted dendritic arrays which are oriented near the symmetric anisotropy directions, consistent with experiments [15]. We found that the transition is characterized through a broadening of the local interface velocity distribution. Specifically, pure seaweed exhibit a narrow transverse velocity distribution near $v_x \approx 0$. Oriented dendritic arrays, which gradually emerge when the thermal gradient is lowered below a certain value, display distinct shoulders in their transverse distribution. A semianalytical theory of the transition was derived, yielding a $G_m$-$v_p$ phase diagram for the crossover between seaweed and dendritic states for low $v_p$.

This work was supported by the Natural Sciences and Engineering Research Council of Canada and The Center for Automotive Materials and Manufacturing. We thank SHARC-NET and the Materials and Manufacturing Research Institute of McMaster University for supercomputer time.

[1] D. Askeland, *The Science of Materials and Engineering* (Thomson Brooks/Cole, Belmont, CA, 2003).
[2] W. Callister, *Materials Science and Engineering an Introduction* (Wiley, New York, 2003).
[3] E. Ben-Jacob, N. Goldenfeld, B. G. Kotliar, and J. S. Langer, Phys. Rev. Lett. **53**, 2110 (1984).
[4] D. A. Kessler and H. Levine, Phys. Rev. A **31**, 1712 (1985).
[5] W. W. Mullins and R. F. Sekerka, J. Appl. Phys. **35**, 444 (1964).
[6] S. Akamatsu, G. Faivre, and T. Ihle, Phys. Rev. E, **51**, 4751 (1995).
[7] J. Bechhoefer and A. Libchaber, Phys. Rev. B **35**, 1393 (1987).
[8] J.-M. Flesselles, A. J. Simon, and A. J. Libchaber, Adv. Phys. **40**, 1 (1991).
[9] J. S. Kirkaldy, L. X. Liu, and A. Kroupa, Acta Metall. Mater. **43**, 2905 (1995).
[10] L. X. Liu and J. S. Kirkaldy, Acta Metall. Mater. **43**, 2891 (1995).
[11] W. Losert, O. N. Mesquita, J. M. A. Figueiredo, and H. Z. Cummins, Phys. Rev. Lett. **81**, 409 (1998).
[12] W. Losert, B. Q. Shi, and H. Z. Cummins, Proc. Natl. Acad. Sci. U.S.A. **95**, 431 (1998).
[13] W. Losert, B. Q. Shi, and H. Z. Cummins, Proc. Natl. Acad. Sci. U.S.A. **95**, 439 (1998).
[14] R. Trivedi and K. Somboonsuk, Mater. Sci. Eng. **65**, 65 (1984).
[15] B. Utter, R. Ragnarsson, and E. Bodenschatz, Phys. Rev. Lett. **86**, 4604 (2001).
[16] S. R. Coriell, G. B. McFadden, and R. F. Sekerka, Annu. Rev. Mater. Sci. **15**, 119 (1985).
[17] B. Grossmann, K. Elder, M. Grant, and M. Kosterlitz, Phys. Rev. Lett. **71**, 3323 (1993).
[18] D. A. Kessler and H. Levine, Phys. Rev. A **39**, 3041 (1989).
[19] P. Kopczynski, W.-J. Rappel, and A. Karma, Phys. Rev. E **55**, 1282 (1997).
[20] N. Provatas and J. Dantzig, *The Enyclopedia of Materials Science and Technology* (World Scientific, Oxford, 2001).
[21] T. Ihle and H. Muller-Krumbhaar, Phys. Rev. Lett. **70**, 3083 (1993).
[22] R. Almgren, SIAM J. Appl. Math. **59**, 2086 (1999).
[23] A. Karma, Phys. Rev. Lett. **87**, 115701 (2001).
[24] A. Karma and W.-J. Rappel, Phys. Rev. E **53**, 3017 (1995).
[25] N. Provatas, J. Dantzig, and N. Goldenfeld, Phys. Rev. Lett. **80**, 3308 (1998).
[26] N. Provatas (unpublished). This analysis follows [22] using, however, a variable interface definition $-1 < \phi_o < 1$ and expanding in $\delta = W_o V_s/D$ and $\kappa W_o$ analogously to Ref. [27].
[27] K. R. Elder, Martin Grant, Nikolas Provatas, and Mike Kosterlitz, Phys. Rev. E **64**, 1604 (2001).
[28] N. Provatas, J. Dantzig, and N. Goldenfeld, J. Comput. Phys. **148**, 265 (1999).
[29] Y. Saito, C. Misbah, and H. Muller-Krumbhaar, Phys. Rev. Lett. **63**, 2377 (1989).
[30] J. D. Hunt and K. A. Jackson, Metall. Trans. **236**, 843 (1966).